Impacts of Air–Sea Coupling on the Simulation of Mean Asian Summer Monsoon in the ECHAM4 Model*

XIOUHUA FU, BIN WANG, AND TIM LI

International Pacific Research Center, School of Ocean and Earth Science and Technology, University of Hawaii at Manoa, Honolulu, Hawaii

(Manuscript received 10 July 2001, in final form 1 April 2002)

ABSTRACT

Atmosphere–ocean coupling was found to play a critical role in simulating the mean Asian summer monsoon and its climatological intraseasonal oscillation (CISO) in comparisons of the results from a stand-alone ECHAM4 atmospheric general circulation model (AGCM) and a coupled ECHAM4–ocean [Wang–Li–Fu (WLF)] model. The stand-alone simulation considerably overestimates the equatorial Indian Ocean rainfall and underestimates monsoon rainfall near 15°N, particularly over the eastern Arabian Sea and the Bay of Bengal. Upon coupling with an ocean model, the simulated monsoon rainfall becomes more realistic with the rainbelt near 15°N (near the equator) intensified (reduced). These two rainbelts are connected by the northward-propagating CISOs that are significantly enhanced by the air–sea interactions.

Both local and remote air–sea interactions in the tropical Indian and Pacific Oceans contribute to better simulation of the Asian summer monsoon. The local impact is primarily due to negative feedback between SST and convection. The excessive rainfall near the equatorial Indian Ocean reduces (increases) the downward solar radiation (upward latent heat flux). These changes of surface heat fluxes cool the sea surface upon coupling, thus reducing local rainfall. The cooling of the equatorial Indian Ocean drives an anticyclonic Rossby wave response and enhances the meridional land–sea thermal contrast. Both strengthen the westerly monsoon flow and monsoon rainfall around 15°N. The local negative feedback also diminishes the excessive CISO variability in the equatorial Indian Ocean that appeared in the stand-alone atmospheric run. The remote impact stems from the reduced rainfall in the western Pacific Ocean. The overestimated rainfall (easterly wind) in the western North (equatorial) Pacific cools the sea surface upon coupling, thus reducing rainfall in the tropical western Pacific. This reduced rainfall further enhances the Indian monsoon rainfall by strengthening the Indian–Pacific Walker circulation. These results suggest that coupling an atmospheric model with an ocean model can better simulate Asian summer monsoon climatology.

1. Introduction

Sperber and Palmer (1996) have suggested that realistic simulations of climatological mean Asian summer monsoon rainfall will improve the predictability of its interannual variability. However, most of the present atmospheric general circulation models (AGCMs) have a variety of problems in producing a realistic mean Asian summer monsoon (Gadgil and Sajani 1998). This suggests that our understanding of the physical processes that determine the mean Asian summer monsoon is not good enough to warrant a realistic simulation of monsoon rainfall climatology.

Webster (1987) indicated that the differential response of land and ocean to the annual cycle of solar radiation establishes a north–south thermal gradient, which is the fundamental cause of the Asian summer monsoon. Further, Yang et al. (1992) showed that there are three principal circulation cells associated with the south Asian summer monsoon: the lateral and transverse monsoons and the Indian–Pacific Walker circulation. Those divergent circulations are largely driven by the latent heat and radiative heating gradient. The importance of orography in determining the characteristics of monsoons and shaping the rainfall distribution has been demonstrated by a number of numerical experiments (Hahn and Manabe 1975; Kuo and Qian 1981). Though the heating of the landmass is generally considered to be the most important force of the monsoon system, Shukla and Fennessy (1994) found that the annual SST cycle in the Indian Ocean is also a significant factor.

* School of Ocean and Earth Science and Technology, University of Hawaii at Manoa Publication 6002 and International Pacific Research Center Publication 161.

Corresponding author address: Dr. Xiouhua Fu, IPRC, SOEST, University of Hawaii, 2525 Correa Road, Honolulu, HI 96822.
E-mail: xfu@soest.hawaii.edu

© 2002 American Meteorological Society

Gadgil and Sajani (1998) compared monthly mean precipitation of 31 AGCMs in the Atmospheric Model Intercomparison Project I (AMIP I) project and found that only a few models are able to reasonably simulate the mean summer monsoon rainfall in the Indian sector. In boreal summer, two rainbelts are observed, located around 15°N (called the Indian monsoon rainbelt) and the equatorial Indian Ocean, respectively. However, most models overestimate one of them while underestimating the other.

One peculiar characteristic of the Asian summer monsoon is the annual phase locking of the transient intraseasonal oscillation, which has been called the climatological intraseasonal oscillation (CISO) by Wang and Xu (1997) and Kang et al. (1999). Kang et al. (2002, hereafter referred to as KJW02) showed that the two rain belts in the south Asian summer monsoon are connected by the northward-propagating CISOs. Wang and Xu (1997) and Kang et al. (1999) also documented the northward-propagating CISOs over the western North Pacific and Indian regions. However, AGCMs have difficulty in reproducing this phenomenon (Kang et al. 2002). The common deficiencies of AGCMs in simulating the mean Asian summer monsoon and its CISO suggest that some physical processes are misrepresented in AGCMs or missing in the simulations with standalone AGCMs.

Monsoon–ocean interaction has been found to play an important role in the interannual variability of Asian monsoons. Wang et al. (2000) pointed out that the warm pool air–sea interaction provides a positive thermodynamic feedback, which maintains the western North Pacific anomalies, exerting a prolonged influence of ENSO on the east Asian summer monsoon. Lau and Nath (2000) found that the air–sea interaction in the Indian Ocean acts to offset the remote impacts of ENSO on the Indian summer monsoon. However, the possible impacts of air–sea coupling in the tropical Indian and Pacific Oceans on regulating the climatology of the Asia–Pacific summer monsoon are rarely explored. Because the atmospheric circulations associated with the mean Asia–Pacific summer monsoon cover large parts of the tropical Indian and Pacific Oceans, air–sea coupling very likely plays some role in this giant monsoon system. On the one hand, the SST annual cycle in the tropical Indian Ocean is regulated by the Indian monsoon activities (McCreary et al. 1993); on the other hand, the SST annual cycle has a considerable impact on the Indian monsoon (Shukla and Fennessy 1994). Regarding the interactions between the Asian summer monsoon and tropical Pacific Ocean, the ENSO–monsoon relationship on interannual timescales has been an active research topic for a long time (Rasmusson and Carpenter 1983; Ju and Slingo 1995). On annual timescales, however, the interactions are not well understood, though some studies (Meehl 1987; Yang et al. 1992; Murakami and Wang 1993) indicate that the Asian summer monsoon and tropical Pacific Ocean are connected together through the large-scale east–west atmospheric circulation.

In this paper, the impacts of air–sea coupling in the tropical Indian and Pacific Oceans on simulating the mean Asian summer monsoon and its CISO are explored with numerical experiments. The models used are the ECHAM4 AGCM and its hybrid coupled version with the WLF (Wang–Li–Fu) intermediate upper-ocean model (Wang et al. 1995; Fu and Wang 2001). In the following section, the hybrid coupled model and its two components (ECHAM4 AGCM and WLF intermediate ocean model) are introduced. Section 3 compares the climatological aspects of the Asian summer monsoon simulated in the stand-alone ECHAM4 and the coupled model. Section 4 discusses the specific roles of atmosphere–ocean coupling in the tropical Indian Ocean and Pacific Ocean on regulating the Asian summer monsoon. Summary and discussions are in section 5.

2. Model description

a. The ECHAM4 atmospheric model

The atmospheric model used in this study is the ECHAM4 general circulation model, which has been documented in detail by Roeckner et al. (1996). A brief description is given here for the convenience of readers. We used the T30 version (the corresponding horizontal resolution is about 3.75°) instead of the standard ECHAM4 T42 version in this study, because it produces similar results as the higher-resolution versions but requires less computational resources (Stendel and Roeckner 1998). The model has 19 layers extending from the surface to 10 hPa. Its land surface scheme is a modified bucket model with improved parameterization of rainfall-runoff (Dumenil and Todini 1992). The surface fluxes of momentum, heat, water vapor, and cloud water are based on the Monin–Obukhov similarity theory. The vertical diffusion in the model is computed with a high-order closure scheme depending on the turbulent kinetic energy. Gravity wave drag associated with orographic gravity waves is simulated after Miller et al. (1989). The mass flux scheme of Tiedtke (1989) for deep, shallow, and midlevel convection has been used with the modified closure schemes for penetrative convection and the formation of organized entrainment and detrainment (Nordeng 1995). The radiation scheme is a modified version of the European Centre for Medium-Range Weather Forecasts (ECMWF) scheme. Two- and six-band intervals are used in the solar and terrestrial part of the spectrum, respectively.

b. The WLF intermediate upper-ocean model

The WLF model is a tropical upper-ocean model with intermediate complexity. It was originally developed by Wang et al. (1995) for the tropical Pacific and improved by Fu and Wang (2001). The WLF model comprises a

TABLE 1. Numerical experimental designs.

Properties Expt symbols*	Running mode	Atmosphere–ocean coupling region
ECHAM4	Stand-alone	No
Coupled	Coupled	Indian and Pacific Oceans
Indian	Coupled	Indian Ocean
Pacific	Coupled	Pacific Ocean
NO_ECP	Coupled	Indian and western Pacific Oceans**

* The symbols used in the figures.
** The western Pacific here means the tropical oceanic region west of the dateline.

mixed layer, in which the temperature and velocity are vertically uniform, and a thermocline layer in which temperature decreases linearly from the mixed-layer base to the thermocline base. Both layers have variable depths. The deep ocean beneath the thermocline base is motionless with a constant reference temperature. The entrained water temperature is parameterized in terms of the vertical temperature gradient between the mixed layer and the deep inert layers. The mixed-layer turbulence parameterization follows that of Gaspar (1988), which treats the penetrated solar radiation in a more realistic fashion. The WLF model reproduces well the annual cycles of sea surface temperature, upper-ocean currents, and mixed-layer depth in the tropical Pacific (Fu and Wang 2001; Wang and Fu 2001).

In this study, the ocean model has been extended to include both the tropical Indian Ocean and Pacific Ocean (from 30°S to 30°N) with realistic but simplified coastal boundaries of the oceans. The standard spatial resolution of the model is 2° longitude by 1° latitude, which requires an approximate time interval of 3 h. No-flux conditions for temperature and no-slip conditions for velocities are applied at the coastal boundaries.

c. The coupling scheme and experimental design

The ECHAM4 was coupled with the WLF ocean model in the tropical Indian and Pacific Oceans without heat flux correction. Beyond the coupling regions, the underlying sea surface temperature is specified as the climatological monthly mean of the 16-yr (1979–94) SST dataset used as the boundary conditions in the AMIP II experiments (Taylor et al. 2000).

The atmospheric component exchanges information with the ocean component once a day. The atmosphere provides daily mean surface winds and heat fluxes to the ocean model. The latter send daily mean SST back to the former. The coupled model is integrated with seasonally varying solar radiation forcing. The initial atmospheric field is from the ECMWF analysis on 1 January 1988. The initial ocean field is the steady state in January of 10-yr integrations of the ocean model with observed climatological surface winds and heat fluxes. Five experiments were conducted for this study (Table 1). All the experiments were integrated for 16 yr. The outputs of the last 10 yr were used to construct the climatological means in the analyses that follow below.

3. Asia–Pacific summer monsoon in the ECHAM4 and the coupled model

a. Mean summer monsoon

Roeckner et al. (1996) has evaluated comprehensively the performance of the ECHAM4 against the ECMWF analysis data and other observations. Here, we compares only ECHAM4 rainfall and 850-hPa winds in boreal summer (June–July–August–September) with the corresponding observations from the climatological Climate Prediction Center Merged Analysis of Precipitation (CMAP) rainfall data averaged from 1979 to 1998 (Xie and Arkin 1997) and ECMWF-analysis 850-hPa winds averaged from 1985 to 1992. Compared to the observations (Fig. 1a), the simulated Indian monsoon rainfall is weak, whereas the equatorial Indian Ocean rainfall is too strong (Fig. 1c). These deviations in the simulations are associated with an excessive equatorward recurvature of the Somali jet, which may occur because the diabatic processes or frictional effects modify the potential vorticity of the air crossing the equator insufficiently (Rodwell and Hoskins 1995).

In the coupled-model simulation (Fig. 1b), the rainbelt in the equatorial Indian Ocean between the equator and 10°N splits into a northern rainbelt near 15°N and an equatorial rainbelt, as in the observations. The simulated rainfall magnitudes in the Arabian Sea and Bay of Bengal, however, are weaker than in the observations. In both the ECHAM4 and coupled run, the rainfall centers near the South China Sea are shifted eastward and lock onto the Philippines island chain. Rainfall over the equatorial western Pacific in the coupled run is greatly reduced compared to the ECHAM4 result, particularly in the South Pacific convergence zone (SPCZ). The difference in rainfall between the coupled run and the stand-alone run indicates that the tropical air–sea interactions considerably change the Asia–Pacific summer monsoon climatology. The rainfall pattern in the Indian sector becomes more realistic. However, the rainfall over the SPCZ is greatly reduced.

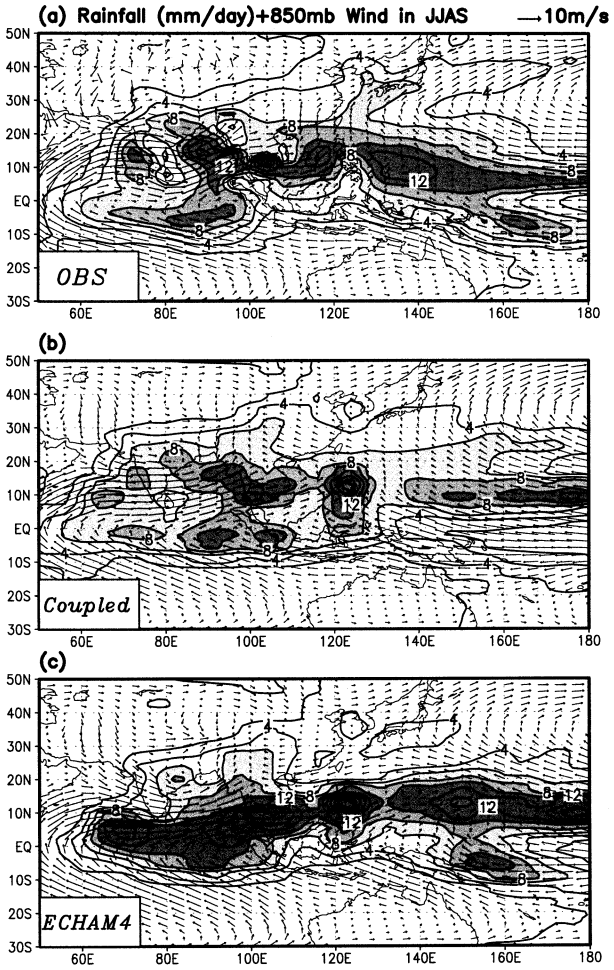

FIG. 1. The mean rainfall rate (mm day^{-1}) and 850-hPa wind vector in boreal summer (Jun, Jul, Aug, and Sep) from the (a) observations, (b) coupled model, and (c) stand-alone ECHAM4. CMAP rainfall (Xie and Arkin 1997) and ECMWF analysis wind fields have been taken as the observations. Contour interval for the rainfall rate is 2 mm day^{-1}.

b. Temporal evolution of the Asian summer monsoon

The simulated pentad-mean rainfall from March to October in the coupled run and stand-alone ECHAM4 run is compared in Fig. 2 with observations along two latitudinal cross sections of 70°–80°E and 80°–100°E. In the observations (Fig. 2a), the rainfall rate exceeds 6 mm day^{-1} at 10°N around pentad 30 along 70°–80°E, representing the summer monsoon onset over the south Indian continent (Anathakrishnan and Soman 1988; Nakazawa 1992). Then rainfall quickly reaches its peak phase at pentad 32. At 20°N, the onset date of the summer monsoon is around pentad 34 and its peak around pentad 42. From pentad 30 to pentad 50, heavy rainfall occurs between 10° and 30°N, corresponding to the rainy season over the Arabian Sea and the western central Indian continent. However, in the ECHAM4 (Fig. 2c), the major rainfall region is confined to south of 10°N, though a wet event near pentad 40 has progressed to 25°N. In the coupled run (Fig. 2b), the summer monsoon rain belt between 10° and 30°N is well simulated with a peak phase around pentad 42, as in the observations. However, the monsoon onset around 10°N is around pentad 33, nearly three pentads later than in the observations. In general, the air–sea coupling improves the simulation of the temporal evolution of the summer monsoon rainfall in the Arabian Sea and western central India.

Figure 2d shows that the observed equatorial rainbelt along the cross section over the Bay of Bengal and East India (80°–100°E) splits into two on pentad 32. These two rain belts persist till the end of September (pentad 55, Fig. 2d). The southern one is located around 5°S and the northern one around 15°N. The two rain belts are connected together by several northward-propagating CISO events. The stand-alone ECHAM4 run produces some rainfall over the Bay of Bengal and East India during boreal summer (Fig. 2f). However, the major rainfall is still concentrated between the equator and 12°N, which is contrary to the observations (Fig. 2d). In contrast, the coupled run (Fig. 2e) simulates the temporal evolution of the summer monsoon rainfall much more realistically. A sporadic rainfall regime similar to the observations develops between the equatorial rainbelt and Indian monsoon rainbelt (~15°N). The northward-propagating CISOs between two major rainbelts are discernible. This signal is barely seen in the simulations of almost all AGCMs participated in the Asian summer monsoon intercomparison project (KJW02).

The abrupt intensification of the western North Pacific (WNP) summer monsoon around pentad 43 has gained the attention of some researchers (Nakazawa 1992; Kawamura and Murakami 1998) because of its possible association with the withdrawal of the Mei-yu/Baiu front in East Asia. This intensification has been reproduced to some extent by both the ECHAM4 and the coupled run. Figure 3 presents the rainfall change from pentad 39 to pentad 43 in the observations, the coupled run, and the ECHAM4. The observed intensification of the WNP monsoon appears as a zonally elongated rainband from 110° to 170°E, centered near 17°N (Fig. 3a). Its north and south sides are two rainfall-decaying regions. The northern dry belt corresponds to the withdrawal of the Mei-yu/Baiu front. Rainfall along 10°N in the Indian sector also decreases in this period. These three dry zones appear to form an elongated ''horseshoe'' around the strong convective zone in the WNP. This feature is similar to the second outgoing longwave radiation (OLR) EOF mode of the observed intraseasonal oscillation in Lau and Chan (1986, their Fig. 7b). The coupled run reproduces all these three dry zones (Fig. 3b), though the rainfall intensification in the WNP is much weaker, particularly near 130°E. In the ECHAM4 (Fig. 3c), the intensification in the WNP is stronger than that in the coupled run. Since the major decaying rainbelt in the Indian sector is located around

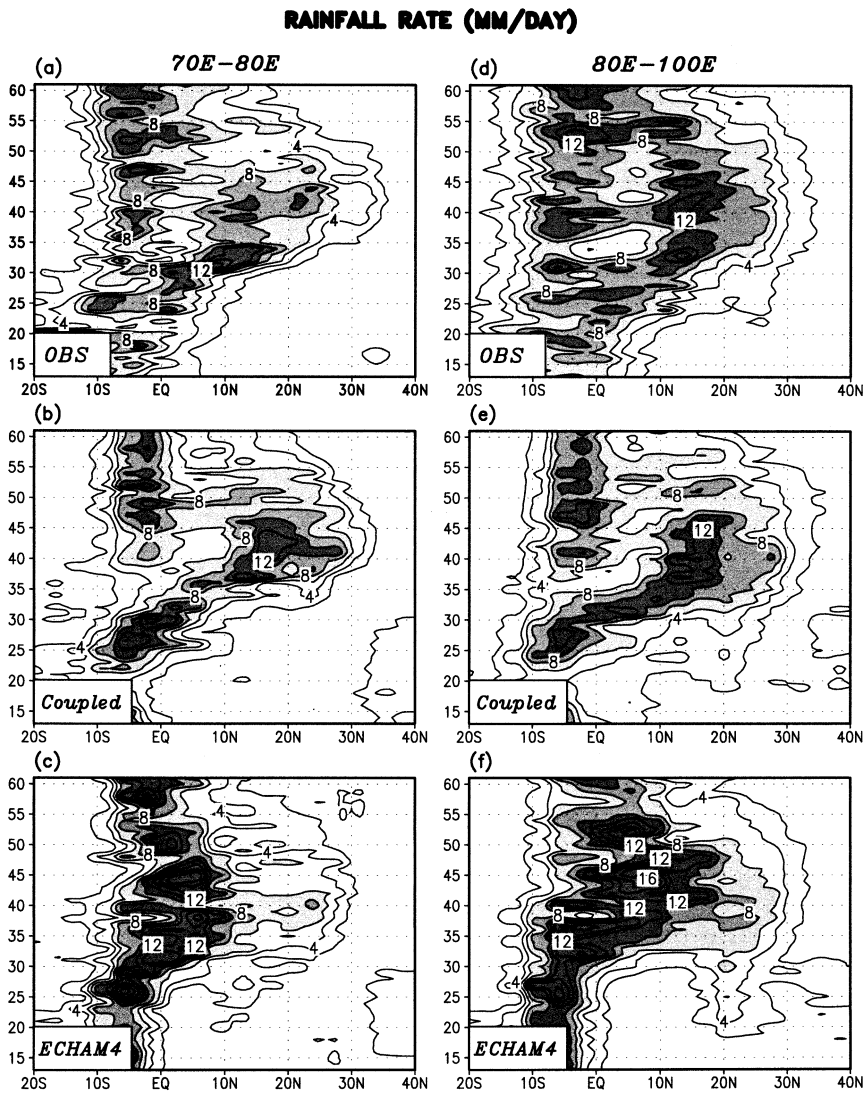

FIG. 2. The time–latitude cross sections of rainfall rate (mm day^{-1}) along 70°–80°E for the (a) observations, (b) coupled model, and (c) stand-alone ECHAM4; the counterparts along 80°–100°E are (d), (e), and (f). The time axis changes from pentad 13 (early Mar) to pentad 61 (early Nov). Contour interval for the rainfall rate is 2 mm day^{-1}.

10°S instead of 10°N, the stand-alone model produces no obvious horseshoe-shaped dry zones as in the observations and the coupled run.

c. Climatological intraseasonal oscillation

The ability of atmospheric models to simulate the CISO of the Asian summer monsoon has been evaluated in 10 AGCMs by KJW02. They found that the AGCMs had difficulties in reproducing the major properties of the CISO (e.g., the timing and propagation route). In the following, we will show that air–sea coupling improves the simulated CISO in several aspects.

Harmonic analysis has been used to extract the CISO signal from the climatological pentad-mean rainfall data. Wang and Xu (1997) found that the dominant period of the CISO is 20–40 days in the equatorial region but 60–70 days in the off-equatorial region. In the following analyses, all the harmonics from 5 to 17 (corresponding to about 20–70 days) have been treated as CISO signals. The variance of CISO has been used to represent the intensity of CISO activity, which is calculated as $(P_{\text{ciso}} \times P_{\text{ciso}})^{0.5}$; where P_{ciso} is the CISO rainfall rate. The results using harmonic analysis for the climatological pentad-mean data and the 10-yr composite of the intraseasonal oscillation of individual years are almost the same. So, the CISO extracted directly from the climatological pentad-mean data is used in the following analyses.

Figure 4 presents the variance of CISO from May to

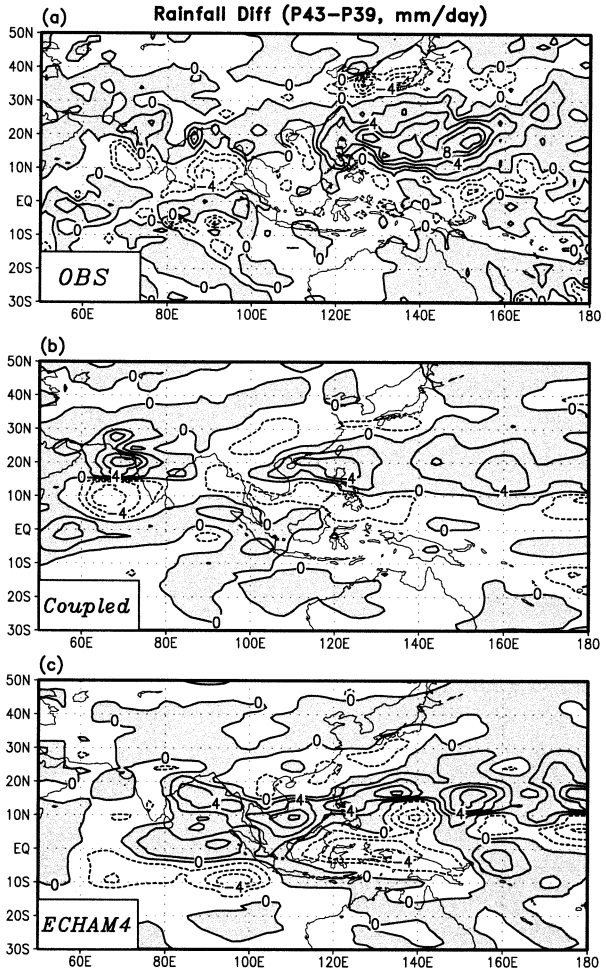

FIG. 3. The changes of rainfall rate (mm day^{-1}) from pentad 39 to pentad 43 for the (a) observations, (b) coupled model, and (c) stand-alone ECHAM4. Contour interval for the rainfall rate is 2 mm day^{-1}.

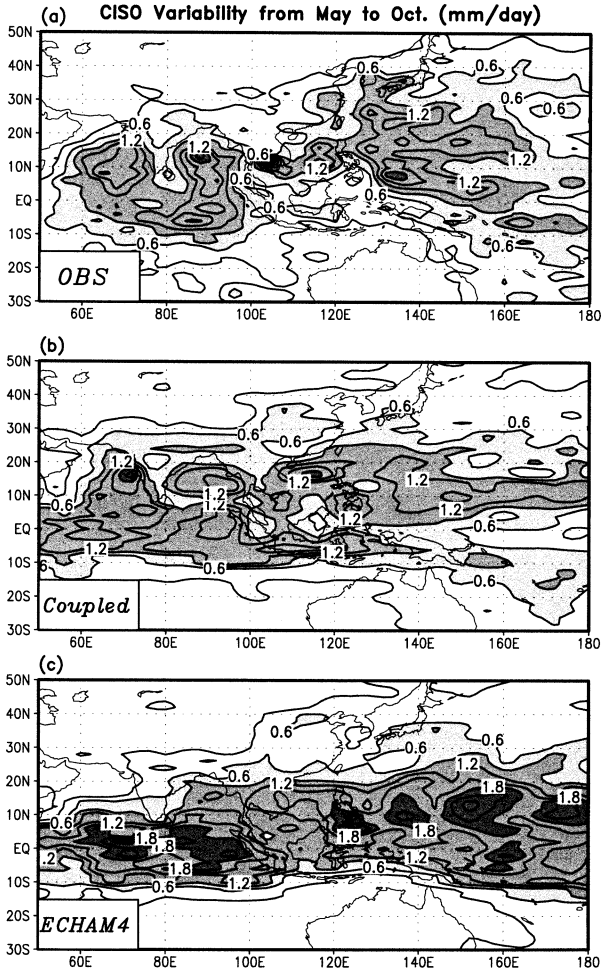

FIG. 4. The variance of climatological intraseasonal oscillation (CISO, filtered) rainfall rate (mm day^{-1}) from May to Oct for the (a) observations, (b) coupled model, and (c) stand-alone ECHAM4. Contour interval is 0.3 mm day^{-1}.

October for the observations, the coupled run, and the ECHAM4. The spatial distributions of the CISO variance and the mean summer monsoon rainfall correlate well (Figs. 4 and 1). The spatial correlation coefficients for the observations, the coupled run, and the ECHAM4 are 0.79, 0.75, and 0.69, respectively. The observed CISO has four major active regions: the WNP, the Bay of Bengal, the Arabian Sea, and the equatorial Indian Ocean. Those regions are reproduced well in the coupled run except that the amplitude is less at the action centers (Fig. 4b). In the ECHAM4, the CISO variance in the western Pacific is similar to the observed variance except that the amplitude is exaggerated and the strong CISO activity extends too far eastward (Fig. 4c). The largest discrepancy occurs in the Indian sector. The major CISO activity in the stand-alone model is too strong and narrowly trapped to the equatorial region. Considering the high spatial correlation between the mean rainfall and the CISO variance in all these cases (the observations, coupled run, and the ECHAM4), the improvement of one of them (seasonal mean rainfall or CISO) may automatically make the other better.

The CISO signals that propagate northward to connect the equatorial rainbelt with the Indian monsoon rainbelt are much better simulated in the coupled run than in the stand-alone ECHAM4 run. Figure 5 shows the latitude–time cross sections of CISO from the CMAP rainfall data, the coupled model, and the ECHAM4 for latitudinal bands 70°–80°E and 80°–100°E. Over the Indian sector, the northward propagation of CISO is primarily observed from April to August (Kang et al. 1999). For clarity, only those data from pentad 19 (early April) to pentad 48 (late August) are presented in the figures. In this period, three major rainfall events in the Arabian Sea and western India can be identified in the observations (Fig. 5a). The strongest event starts near 10°S at pentad 25 and ends up near 20°N at pentad 35, which is associated with the onset of the summer monsoon in the Arabian Sea and western India. Both the coupled run and the

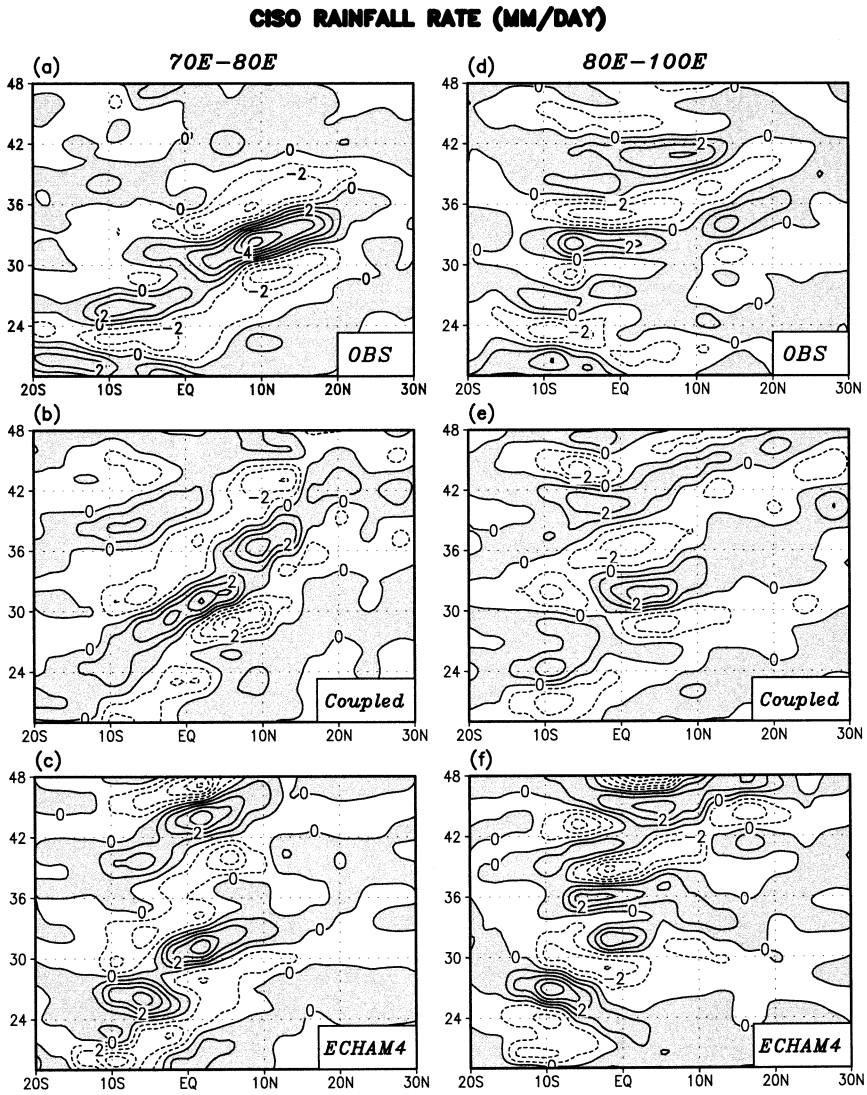

FIG. 5. The time–latitude cross sections of CISO (filtered) rainfall rate (mm day^{-1}) along 70°–80°E for the (a) observations, (b) coupled model, and (c) stand-alone ECHAM4; the counterparts along 80°–100°E are (d), (e), and (f). The time axis changes from pentad 19 (early Apr) to pentad 48 (late Aug). Contour interval for the rainfall rate is 1 mm day^{-1}.

ECHAM4 capture the three events. However, the CISO in the coupled run (Fig. 5b) propagates much farther north than in the ECHAM4. The CISO activities in the stand-alone run are primarily confined to south of 10°N (Fig. 5c). Note also that the northward-propagating speed of CISO in the coupled run is slower than in the observations. The simulated summer monsoon over the Arabian Sea and western India in the coupled run, therefore, has a later onset. Over the Bay of Bengal, two northward-propagating CISO events are discernible from pentad 30 to 45 in the observed rainfall (Fig. 5d). These events have been well reproduced in the coupled run (Fig. 5e). In the ECHAM4 case (Fig. 5f), though several CISO cycles are found near the equatorial Indian Ocean, no systematic northward propagation as that in the observations and coupled run is produced. These results indicate that the CISO signals are present in both the ECHAM4 and the coupled run. However, the northward propagation (in both the Arabian Sea and Bay of Bengal) and timing of the CISO events (particularly in Bay of Bengal) seem much better in the coupled run. The better simulation of the rainfall change in the Indian sector from pentad 39 to pentad 43 (Fig. 3) in the coupled run can be explained by the improvement of the CISO simulations.

Overall, the atmosphere–ocean coupling improves the simulations of mean Asian summer monsoon rainfall (except the underestimated rainfall in the SPCZ) and its climatological intraseasonal oscillation, particularly in

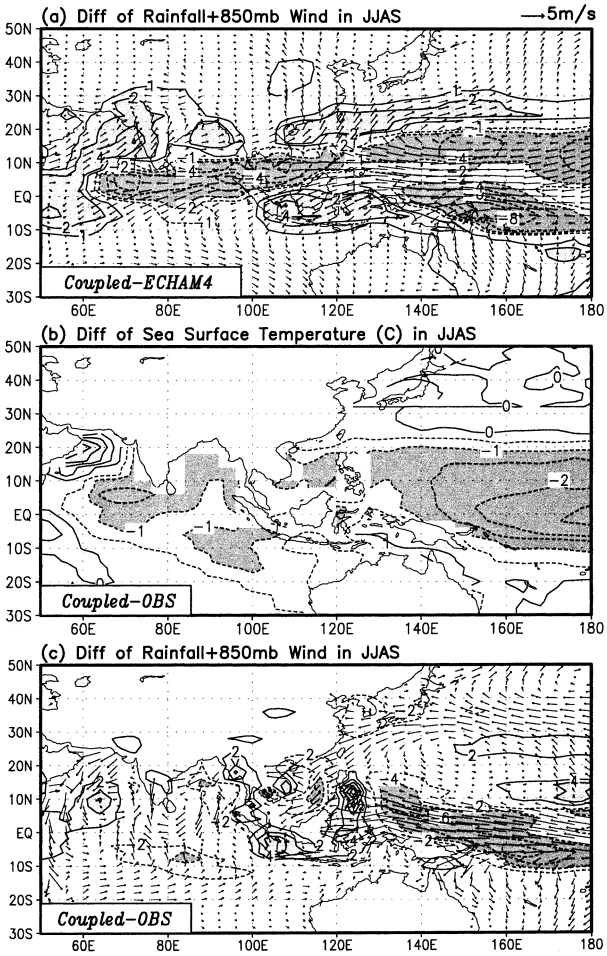

FIG. 6. (a) The differences between the coupled model and the stand-alone ECHAM4 in the rainfall rate (mm day^{-1}) and 850-hPa wind vector (except the contours for 1 and -1, the other contour interval of the rainfall rate is 2 mm day^{-1}). The differences between the coupled model and the observations in (b) SST and (c) rainfall rate (mm day^{-1}) and 850-hPa wind vector (coupled-OBS). The contour interval for SST is 0.5°C; the contour interval for rainfall rate is 2 mm day^{-1} (the zero contour is not drawn).

the Indian sector. The causes of these improvements are explained and further explored with several sensitivity experiments in the following section.

4. Air–sea coupling processes impacting the simulation of the Asian summer monsoon

a. Hypotheses concerning the Indian monsoon improvements in the coupled simulation

Figure 6a shows that the air–sea coupling systematically reduces the rainfall from the Indian Ocean between the equator and 10°N, and increases the rainfall over the Indian monsoon trough, especially over the eastern Arabian Sea and Bay of Bengal. Why is the south Asian summer monsoon rainfall better simulated in the coupled run than in the stand-alone ECHAM4 run? It is important to understand how this has happened.

Our hypothesis is that the coupling overcomes some of the deficiencies inherent in the ECHAM4 model. The enhancement of rainfall in the Indian monsoon region (between 10°–30°N) is partially due to the negative rainfall anomaly near the equatorial Indian Ocean, because this suppressed rainfall anomaly can force an anticyclonic Rossby wave response in the northern Indian Ocean and increases the southwesterly monsoon flow (Fig. 6a), thus leading to a stronger Indian monsoon rainfall. The atmospheric cooling near the equatorial Indian Ocean (Fig. 6b) also enhances the meridional land–sea thermal contrast and pressure gradient, thus strengthening the westerly monsoon flow and monsoon rainfall over the Arabian Sea and Bay of Bengal. In addition, upon coupling, the rainfall in the tropical western Pacific and SST show significant negative anomalies (Figs. 6a and 6b). The reduced rainfall in the western tropical Pacific also contributes to the increases in the Indian monsoon rainfall through enhancing the Indian–Pacific Walker circulation.

Before testing this hypothesis, we should also discuss problems with the coupled run and their causes. First, the negative rainfall anomalies slightly north of the equatorial Indian Ocean and over the western Pacific Ocean in the coupled run are largely associated with the cold SST bias (Fig. 6b). Where does this SST bias come from? We speculate that it most likely originates from the errors in the atmospheric model, in particular in the net downward surface heat flux (Fig. 7a) and the low-level winds (Fig. 7b). In the equatorial Indian Ocean (except the Somali coast), the excessive rainfall in the ECHAM4 model (Fig. 7b) reduces downward solar radiation and increases upward latent heat flux. The resultant net surface heat flux is considerably lower than the observed (Fig. 7a). Upon coupling with the ocean model, the reduced surface heat flux cools the local sea surface and reduces the local rainfall. The lower SST and weaker convection considerably reduce the surface latent heat flux and increase the solar radiation. Both heat flux changes contribute to the improvement of the net surface heat flux in the coupled run (Fig. 8). Therefore, a new equilibrium climate state is established in this air–sea coupled system. The SST over the tropical Indian Ocean is now about 1°C lower than the observed (Fig. 6b). In the southeast Indian Ocean, the excessive convection over the equatorial Indian Ocean in the stand-alone run seems to enhance the southeast trades (Fig. 7b), thus increasing the latent heat loss and reducing the net downward surface heat flux (Fig. 7a). The coupling decreases the SST over the southeast Indian Ocean (Fig. 6b). The pattern correlation coefficient between the net surface heat flux error (Fig. 7a) and the SST bias (Fig. 6b) in the Indian Ocean and maritime marginal seas (40°–120°E) is as high as 0.78. In the western Pacific, the cold SST bias in the coupled model is believed to originate also from

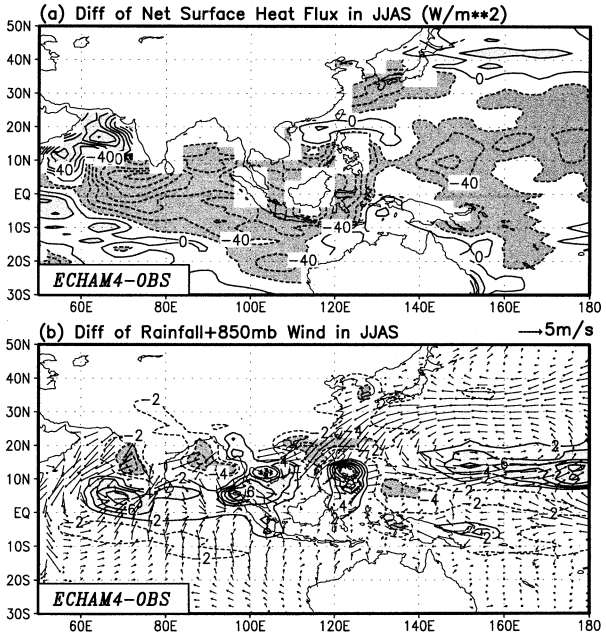

FIG. 7. Discrepancies of the ECHAM4 model results with the observations (OBS) in JJAS, (a) net surface heat flux (W m^{-2}, ECHAM4-OBS, positive means downward), (b) rainfall rate (mm day^{-1}) and 850-hPa wind vector (ECHAM4-OBS). Contour interval for net surface heat flux is 20 W m^{-2}; the contour interval for rainfall rate is 2 mm day^{-1} (the zero contour is not drawn). The observed net surface heat flux is from Oberhuber (1988).

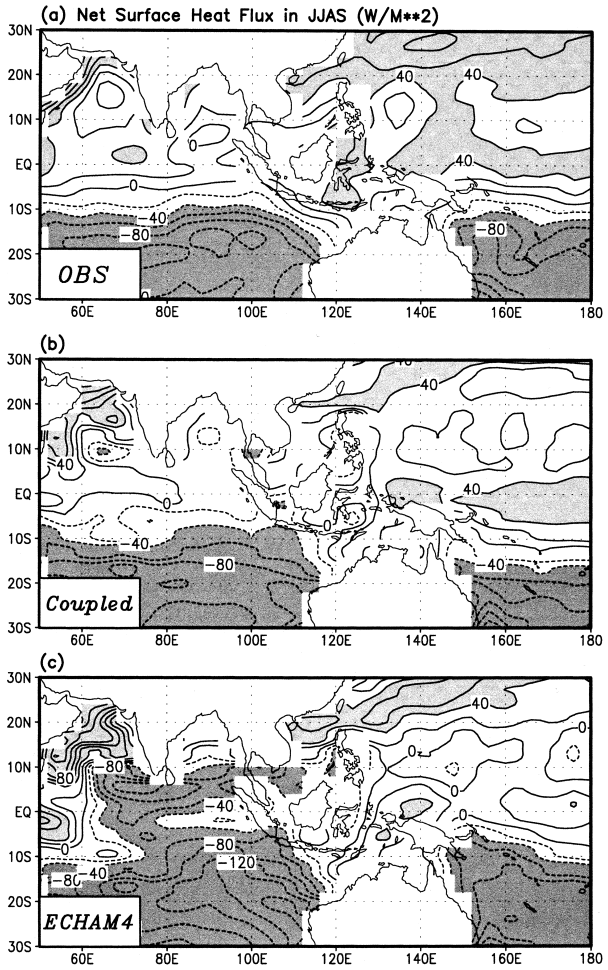

FIG. 8. The mean net surface heat flux (W m^{-2}, positive means downward) in boreal summer (JJAS); (a) the observations, (b) coupled model, and (c) stand-alone ECHAM4. Contour interval is 20 W m^{-2}.

the atmospheric model deficiency and amplified by the dynamic air–sea coupling. Figure 7b shows that between 10°S and 10°N, the ECHAM4 model has excessive easterly winds in the western Pacific, which is due to the exaggerated Walker circulation in the atmospheric model (Roeckner et al. 1996). In addition, the ECHAM model has excessive rainfall in the western North Pacific between 10°–20°N and east of 140°E (Fig. 7b). Upon coupling, in the equatorial western Pacific the enhanced trades reduce the sea surface temperature through increasing entrainment and latent heat flux. Therefore, the new equilibrium state in the coupled run shows the largest negative SST bias (Fig. 6b) in the equatorial western Pacific. The cold SST bias in the western North Pacific (east of 140°E and between 10° and 20°N) is partly attributed to the reduced surface heat flux (Fig. 7a) due to the rainfall bias.

Although the summer monsoon rainfall in south Asia is considerably improved in the coupled run, the SST has a cold bias especially in the western Pacific (Fig. 6b) and the deficient rainfall bias occurs over the SPCZ (Fig. 6c) compared to the observations. One might wonder whether the improved Indian monsoon simulation in the coupled run is a trade-off with the poorer simulation in the SPCZ convection and the cold SST bias in the western Pacific. We note that the deficient rainfall in the SPCZ is associated with the large cold SST bias in this region. Therefore, the remaining concern is whether the improved Indian monsoon simulation is a trade-off with the cold SST bias in the new equilibrium state. We believe that it is not. The cold SST bias in the equatorial western Pacific primarily arises from the air–sea interaction in the central eastern Pacific. We will demonstrate this point shortly, namely, we will show that the cold bias in the western Pacific can be markedly reduced by eliminating the air–sea coupling in the central eastern Pacific, while the simulation of the south Asian summer monsoon remains much improved.

In order to test the aforementioned hypotheses and to address the concern raised in the previous paragraph, three sensitivity experiments were conducted. The basic idea is to isolate the effects of the air–sea coupling in the tropical Indian Ocean, in the Pacific Ocean, and in the warm pool (Indian and western Pacific Oceans). The details of the experimental designs are given in Table 1. In the first experiment (Indian in Table 1), the air–sea coupling is only allowed in the tropical Indian Ocean. In the second experiment (Pacific in Table 1),

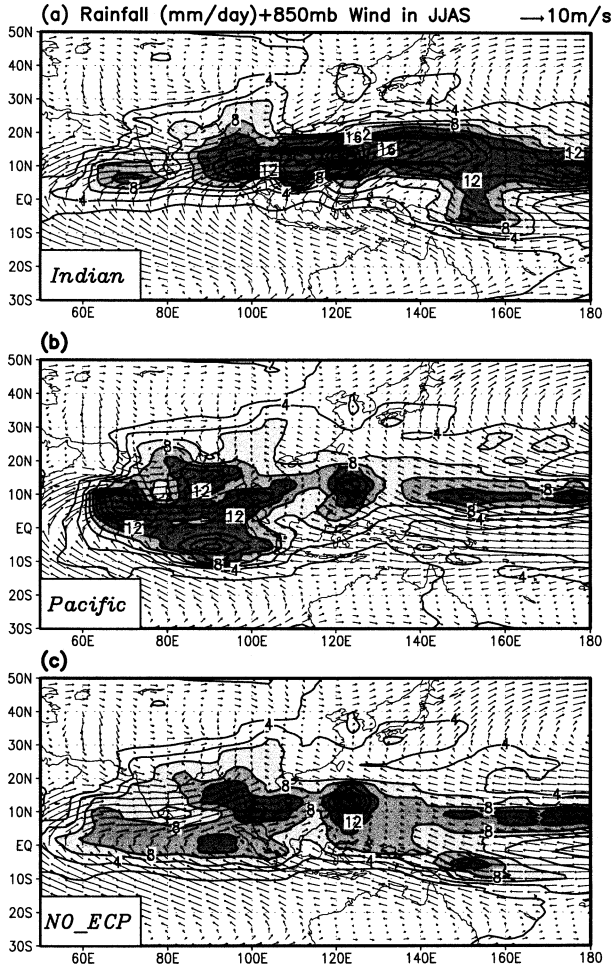

FIG. 9. The mean rainfall rate (mm day^{-1}) and 850-hPa wind vector in boreal summer (JJAS) when only part of Indian and Pacific Oceans is coupled; (a) Indian Ocean only, (b) Pacific Ocean only and (c) Indian and western Pacific Oceans (west of the dateline) only. Contour interval for the rainfall rate is 2 mm day^{-1}.

the air–sea coupling is only activated in the tropical Pacific Ocean. In the last experiment (NO_ECP in Table 1), the air–sea coupling is only active in the tropical Indian Ocean and western Pacific Ocean (west of the dateline). The results from the coupled run discussed in the previous section will be referred as the control run.

b. Effects of air–sea interaction in the tropical Indian Ocean

In this experiment (Indian, Table 1), the air–sea coupling is only activated in the tropical Indian Ocean. The sea surface temperature in other oceanic regions is specified as in the ECHAM4 run. The simulated summer-mean rainfall and 850-hPa winds are shown in Fig. 9a. Compared to the stand-alone ECHAM4 simulation (Fig. 1c), the equatorial monsoon rain belt in the Indian sector occurs further north. This can be seen more clearly in the time–latitude cross sections of 70°–80°E and 80°–100°E (Figs. 10a,d). The largest rainfall in July and August (from pentad 37 to pentad 48) is located between 10° and 20°N rather than between the equator and 10°N in the ECHAM4 (Figs. 2c,f). The northward shift of the major convergence zone is accompanied by decreased rainfall near the equator and increased rainfall north of 10°N (Fig. 11a). However, the largest increase of rainfall is over the South China Sea and the WNP.

As in the control run, the reduced surface heat flux in the ECHAM4 (Fig. 7a) cools the tropical Indian Ocean. The lower SST increases the meridional land–sea thermal contrast, which enhances westerly monsoon flow and rainfall over the Arabian Sea and Bay of Bengal. More moisture (than the ECHAM4 run) is transported into the South China Sea and the WNP, inducing more rainfall there (Murakami et al. 1999). The ascending air mass associated with stronger convection in the western North Pacific tends to descend over the equatorial and southern Indian Oceans, which can be clearly seen from the circulation on the vertical cross section of the southeast Indian Ocean to the WNP (figure not shown).

Though the equatorial convergence zone moves northward in this experiment, the rainfall increases most over the South China Sea and the WNP, not over the northern Indian Ocean. On the other hand, rainfall decreases considerably near the equatorial Indian Ocean, even much more than that in the control run. To understand this result, we may get some clues from the rainfall anomaly dipole in Fig. 11a: the large increase in rainfall over the WNP and the large decrease over the equatorial Indian Ocean. A positive feedback may sustain this tilted rainfall dipole. The enhanced convection in the WNP exports more air in the upper level, which increases subsidence in the equatorial Indian Ocean, suppressing rainfall there. This will intensify the low-level southwesterly from the Indian Ocean into the WNP, further increasing rainfall in the WNP. The lack of air–sea coupling over the WNP excludes negative feedback between local SST and convection, thus producing excessive rainfall. Therefore, in this experiment, the equatorial convergence zone in the Indian sector moves northward as a whole, and does not split into two as in the control run.

The above results indicate that the air–sea coupling in the Indian Ocean partially contributes to the increases of the Indian summer monsoon rainfall in the control run and further suggest that the air–sea coupling over the South China Sea and the WNP is an integral part of the processes that regulate the summer monsoon in the Indian sector.

c. Effects of air–sea interaction in the tropical Pacific Ocean

In this experiment (Pacific, Table 1), air–sea coupling is performed only over the tropical Pacific and maritime

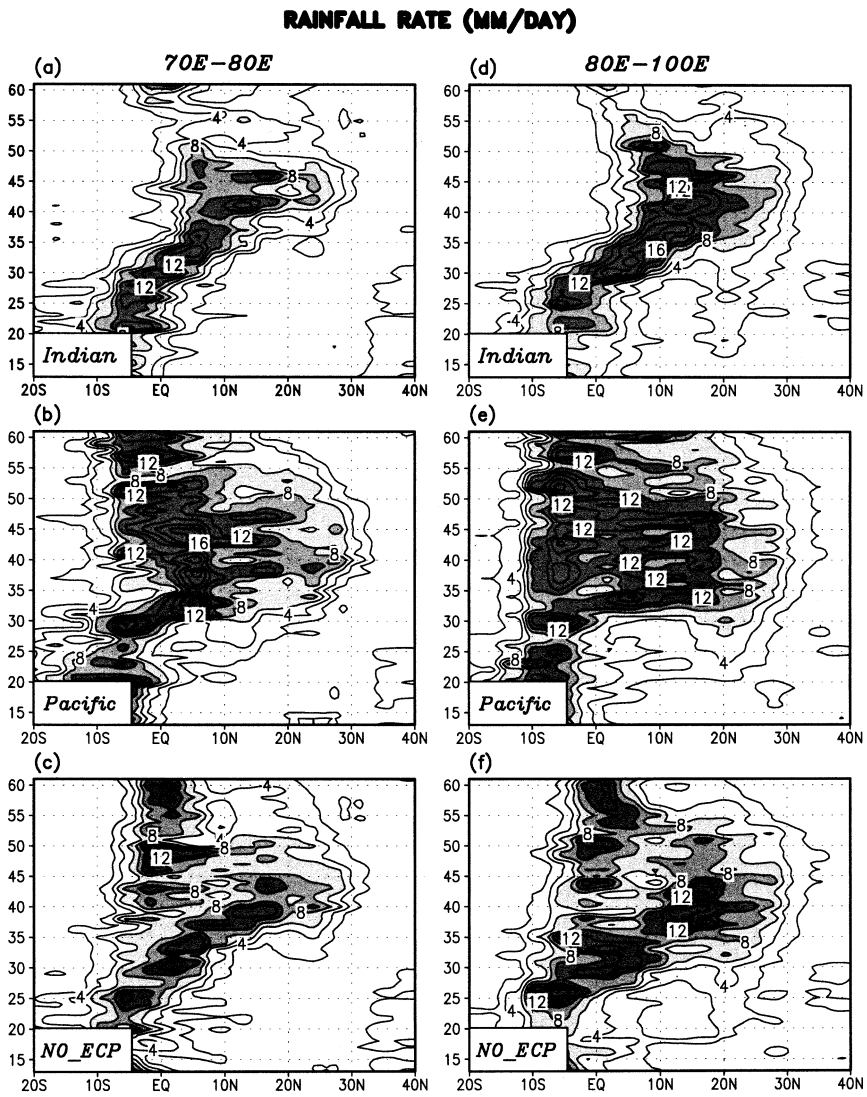

FIG. 10. The time–latitude cross sections of rainfall rate (mm day^{-1}) along 70°–80°E when only part of Indian and Pacific Oceans is coupled; (a) Indian Ocean only, (b) Pacific Ocean only, and (c) Indian and western Pacific Oceans (west of the dateline) only; the counterparts along 80°–100°E are (d), (e), and (f). The time axis changes from pentad 13 (early Mar) to pentad 61 (early Nov). Contour interval for the rainfall rate is 2 mm day^{-1}.

marginal seas. The resulting rainfall in the SPCZ is much less (Fig. 9b) than that in the observation. The rainfall in the Indian sector, on the other hand, is considerably enhanced. But rainfall is not increased near the equator. The largest rainfall appears in the Indian monsoon region (8°–20°N), with a secondary belt just south of the equator (Fig. 12a). The total rainfall over the Indian sector is much larger than that in the ECHAM4 and the observations. The time–latitude cross sections of rainfall over the Indian sector are given in Figs. 10b,e. In boreal summer, the rainfall extends much further north than in the stand-alone run. However, this simulation does not reproduce the relatively weak convective zone between the equator and 10°N in the observations and the control run.

As indicated before, the easterly bias over the western equatorial Pacific in the ECHAM4 considerably cools the western Pacific upon the coupling (Fig. 12b). The lower SST significantly impacts rainfall both locally and remotely. Through decreasing the convective instability and increasing the large-scale divergence, it reduces considerably local rainfall. Its impact on the Indian sector is through changing the large-scale east–west circulation. The cooling of the western Pacific enhances the Indian–Pacific Walker circulation, favoring more convection over the Indian sector. Further, the cooling of the troposphere in the western Pacific expands over the equatorial Indian Ocean (figure not shown) intensifying rainfall both north and south of the equator as shown in Fig. 12a.

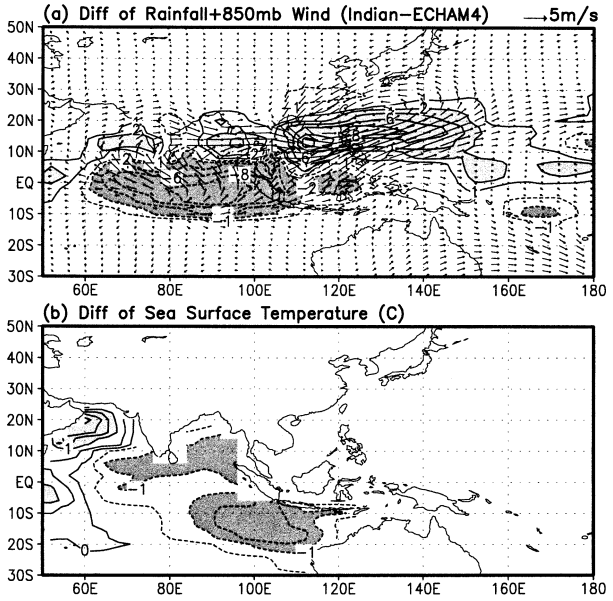

FIG. 11. The differences between the Indian-Ocean-only run and the stand-alone ECHAM4 run; (a) the rainfall rate (mm day^{-1}) and 850-hPa wind vector, and (b) SST. Except the contours for 1 and −1, the other contour interval of the rainfall rate is 2 mm day^{-1}. The contour interval for SST is 0.5°C.

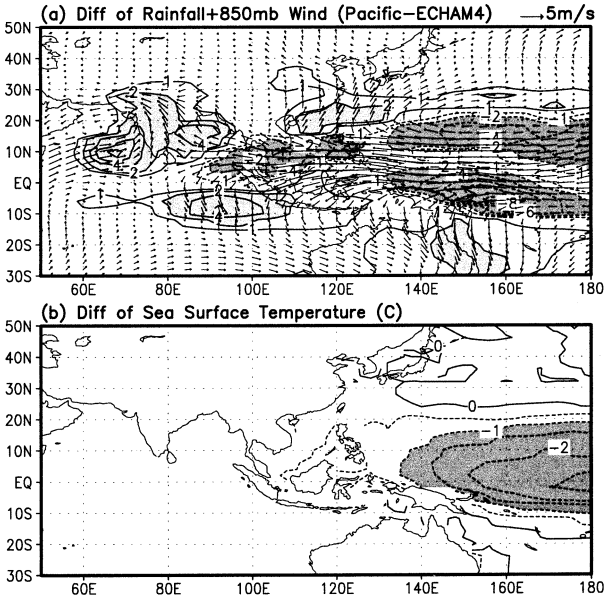

FIG. 12. The differences between the Pacific-Ocean-only run and the stand-alone ECHAM4 run; (a) the rainfall rate (mm day^{-1}) and 850-hPa wind vector, and (b) SST. Except the contours for 1 and −1, the other contour interval of the rainfall rate is 2 mm day^{-1}. The contour interval for SST is 0.5°C.

d. Effects of air–sea interaction in the tropical Indian and western Pacific Oceans

In this run (NO_ECP, Table 1), air–sea coupling is performed for both the tropical Indian Ocean and western Pacific Ocean. Different from the control run, the SST over the central eastern Pacific in this case has been specified as that in the ECHAM4 run. The resultant summer-mean rainfall over the Indian sector (Fig. 9c) is similar to that in the control run. However, the rainfall over the SPCZ becomes much more realistic. The rainfall and 850-hPa winds in the present run deviate the least from the observations (Fig. 13) compared to the stand-alone run and the control run (Figs. 7b and 6c). This result suggests that the mean summer monsoon rainfall in the Asia–Pacific region is best simulated when the air–sea coupling is allowed over the tropical Indian Ocean and western Pacific Ocean.

Time evolution of rainfall along two meridional bands, 70°–80°E and 80°–100°E (Figs. 10c,f), is similar to the observations and to that in the control run. Two rainbelts developed in boreal summer. One is near the equator, and the other is between 10° and 20°N. Two convergence zones are connected to each other by the northward-propagating CISOs.

The differences in the summer rainfall, 850-hPa wind, and SST between this run and the ECHAM4 are shown in Fig. 14. The overall rainfall perturbation is very similar to that in the control run (Fig. 6a) except for smaller negative rainfall perturbation in the SPCZ. This result suggests that the better simulation of summer monsoon rainfall over the Indian sector in the control run is not primarily due to the degraded performance over the SPCZ. The SST change in this case (Fig. 14b) is also very similar to that in the control run. However, the cold bias is much smaller in the equatorial western Pacific. This indicates that a large part of the SST error over the western Pacific in the control run is associated with the dynamic air–sea coupling in the central eastern Pacific. Same as in the control run, the SST change in this case can be largely explained by the errors of net surface heat flux in the ECHAM4 (Fig. 7a). In the equatorial western Pacific, the larger easterly wind in the atmospheric model is responsible for the colder sea surface there, though it is much smaller than that in the control run.

The better simulation of the south Asian summer

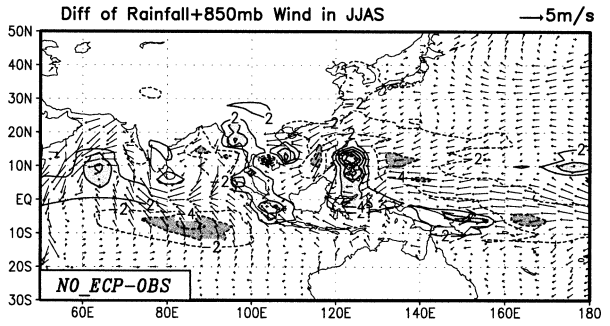

FIG. 13. Discrepancies of rainfall rate (mm day^{-1}) and 850-hPa wind vector between the NO_ECP results with the observations (OBS) in JJAS. Contour interval for rainfall rate is 2 mm day^{-1} (the zero contour is not drawn).

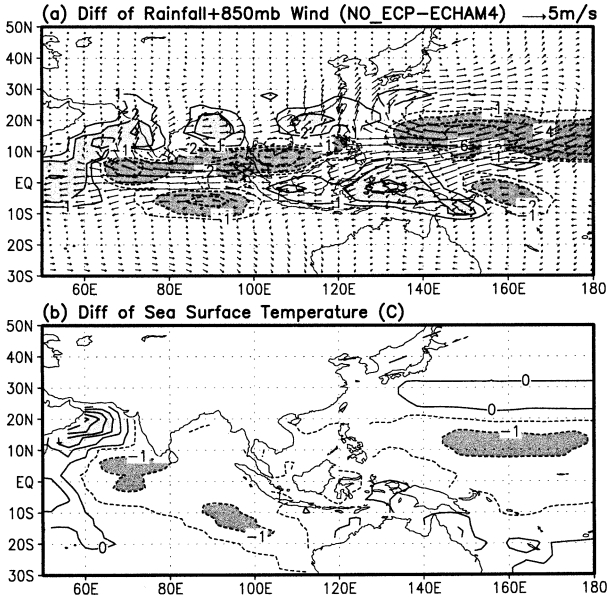

FIG. 14. The differences between the NO_ECP run and the stand-alone ECHAM4 run; (a) the rainfall rate (mm day^{-1}) and 850-hPa wind vector, and (b) SST. Except the contours for 1 and -1, the other contour interval of the rainfall rate is 2 mm day^{-1}. The contour interval for SST is 0.5°C.

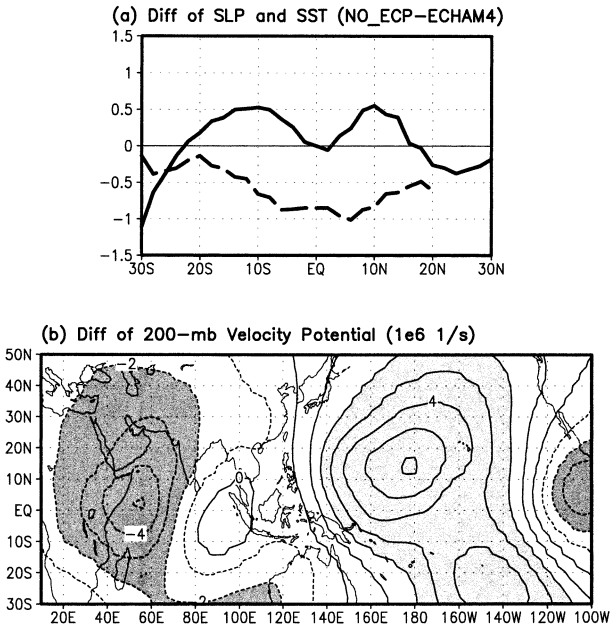

FIG. 15. The differences of sea level pressure (SLP, solid line, unit: hPa) and SST (dash line, unit: °C) averaged between 70° and 100°E, and (b) 200-hPa velocity potential (10^6 s^{-1}) between the NO_ECP run and the ECHAM4 in JJAS. Contour interval for the velocity potential is 1×10^6 s^{-1}.

monsoon in this experiment, comparing with the stand-alone ECHAM4, is caused by the local air–sea coupling in the Indian Ocean and the remote effect from the western Pacific. The excessive rainfall over the equatorial Indian Ocean in the ECHAM4 considerably reduces the downward surface heat flux. Upon coupling with the ocean, the SST is decreased. The lower SST reduces the local rainfall and increases the local sea level pressure (Fig. 15a). This enhances the meridional pressure gradient, thus strengthening the westerly monsoon flow and the Indian monsoon rainfall. An anticyclonic Rossby wave response to the equatorial negative rainfall anomaly (Fig. 14a) also contributes to the intensifications of the southwesterly monsoon flow and Indian monsoon rainfall. On the other hand, the cooling in the western Pacific decreases the rainfall there. A seesaw pattern is developed in the tropical Indian–Pacific region, which can be seen on the 200-hPa velocity potential field (Fig. 15b). The subsidence anomaly in the western Pacific tends to favor the enhancement of convection in the Indian sector.

5. Summary and discussions

a. Summary

After comparing the results between the ECHAM4 run and the coupled run and conducting several sensitivity experiments, we conclude that air–sea coupling in the tropical Indian and western Pacific Oceans plays an important role in rectifying the simulation of the mean Asian summer monsoon rainfall and its climatological intraseasonal oscillation (CISO) in the ECHAM4 model.

In boreal summer, strong rainfall is observed over the eastern Arabian Sea, the Bay of Bengal, and the equatorial Indian Ocean. The ECHAM4 model, however, generates excessive rainfall over the equatorial Indian Ocean, and very weak rainfall in the Arabian Sea and Bay of Bengal. The exaggeration of equatorial Indian Ocean rainfall can be seen in many other AGCMs (Gadgil and Sajani 1998). After coupling ECHAM4 with the WLF ocean model in the tropical Indian and Pacific Oceans, the excessive equatorial Indian Ocean rainfall in the stand-alone case has been reduced, while the rainfall over the Arabian Sea and Bay of Bengal is obviously intensified. The resultant rainfall distribution is similar to the observations. Not only has the general rainfall pattern of mean Asian summer monsoon rainfall been improved, but the coupled run also improves the CISO. In the stand-alone run, the CISO was too strong in the equatorial Indian Ocean. The coupling, on the one hand, reduces the CISO variability to a more realistic magnitude at the equator and, on the other hand, significantly enhances the CISO over the Arabian Sea and Bay of Bengal. The northward propagation of CISOs, which connects the equatorial rainbelt with the monsoon rainbelt, has also been significantly enhanced in the coupled run.

The improved simulation of the mean Asian summer monsoon rainfall and its CISO are largely caused by the adjustment of SST to the errors of the atmospheric mod-

el in the monsoon–ocean interactive system. Associated with the excessive rainfall over the equatorial Indian Ocean in the ECHAM4, the local downward surface heat flux is considerably reduced. Upon coupling, the SST is decreased, which reduces the local rainfall. This negative rainfall anomaly, on the one hand, induces an anticyclonic Rossby wave response in the northern Indian Ocean; on the other hand, it raises sea level pressure in the equatorial Indian Ocean and enhances the meridional land–sea pressure gradient. Both intensify southwesterly monsoon flow and rainfall over the Arabian Sea and the Bay of Bengal. Local negative feedback between SST and convection also diminishes the excessive CISO variability in the equatorial Indian Ocean and western North Pacific. The excessive rainfall and easterly wind anomaly in the ECHAM4 model over the WNP and equatorial Pacific decrease the western Pacific SST through reducing the net surface heat flux and increasing the entrainment after coupling with the ocean model, reducing regional rainfall. The lower SST and reduced rainfall over the western Pacific further enhance the Indian monsoon rainfall through strengthening the Indian–Pacific Walker circulation.

The effects of the air–sea coupling from the tropical Indian Ocean and Pacific Ocean have been demonstrated with two sensitivity experiments, in which air–sea coupling is only active in one ocean basin (Indian and Pacific in Table 1). When air–sea coupling is active in both Indian and Pacific Oceans (coupled, Table 1), the equatorial western central Pacific becomes excessively cold and the rainfall in this region is severely degraded. One may speculate that the improvement of the Indian summer monsoon simulation is primarily a trade-off with the worsening simulation in the western Pacific. Therefore, another sensitivity experiment in which air–sea coupling is only active in the Indian Ocean and western Pacific Ocean (NO_ECP, Table 1) is conducted. In this case, the resultant SST bias in the western equatorial Pacific is very small. The simulated summer monsoon is similar to that in the coupled run over the Indian sector and more realistic over the western Pacific. This result indicates that it is the air–sea coupling in the tropical Indian Ocean and western Pacific Ocean that significantly improves the simulation of the mean Asia–Pacific summer monsoon rainfall. The improvement of the Indian summer monsoon simulation is not a trade-off with the worsening simulation in the western Pacific. The much better simulation of the Indian summer monsoon in this experiment than that in the Indian-Ocean-only case (Indian, Table 1) also suggests the importance of air–sea coupling in the South China Sea and western Pacific on shaping the Indian summer monsoon.

b. Discussions

Though we showed that the air–sea coupling in the tropical Indian Ocean and western Pacific Ocean is able to rectify some major weaknesses of the Asian summer monsoon rainfall simulations in the stand-alone ECHAM4, the improvement is primarily due to the lower SST in the coupled run. One may ask: Is this improvement of the monsoon rainfall due to a wrong reason? Or is the air–sea coupling possibly a significant mechanism to regulate the Asian summer monsoon system?

The main point of this study is that the SST change in the coupled system is primarily a response to the errors of the atmospheric model. In other words, air–sea coupling will change the mean Asian summer monsoon through adjusting the SST according to the errors of the atmospheric model. In this specific coupling system the new equilibrium climate state has cold SST bias. However, for those AGCMs with excessive rainfall in the Indian monsoon region and weak rainfall near the equator (Gadgil and Sajani 1998), air–sea coupling may result in a new equilibrium state with warm SST bias in the equatorial Indian and western Pacific Oceans. The underlying physics is similar to that presented earlier but with reversed sign. The negative and positive net surface heat flux anomalies associated with the errors of atmospheric rainfall would decrease the SST in the Arabian Sea and Bay of Bengal and increase the SST near the equator upon coupling. The changes of convective instability and meridional land–sea pressure gradient may increase rainfall near the equator and reduce rainfall around 15°N, thus generating two convective zones as those in the observations. Regarding the possible remote impacts from the western Pacific, the weak rainfall over the equatorial Indian Ocean may induce a westerly wind anomaly in the equatorial western Pacific. The decrease of the easterly wind in the western Pacific may warm the sea surface, enhancing local rainfall. The remote impacts from this positive rainfall anomaly may further reduce rainfall in the Indian monsoon region through weakening the Indian–Pacific Walker circulation.

The observations and other modeling studies also suggest that air–sea coupling may work in the Asia–Pacific region to regulate the summer monsoon rainfall toward the climatological mean. The 21-yr (1979–99) observed CMAP summer-mean monsoon rainfall over the Asia–Pacific region has been examined. In almost every year, the strong rainfall regions are observed over the Arabian Sea, Bay of Bengal, equatorial Indian Ocean, and western North Pacific, although their strengths change year by year. Compared to the simulations of AGCMs (Gadgil and Sajani 1998), it is very clear that the intermodel differences are much larger than the interannual variability observed in the real world. We may attribute this discrepancy to the uncertainties of AGCMs in representing the convection, cloud, land surface processes, and topography. On the other hand, it is also possible that, in nature, the air–sea coupling over the Indian and western Pacific Oceans reduces the monsoon perturbations induced by the external forcings (e.g., Eurasia snow anomaly and ENSO),

regulating the Asian summer monsoon toward the climatological mean. The lack of air–sea coupling in AGCMs may exaggerate the monsoon perturbations caused by model uncertainties and remote forcings. Barnett et al. (1989) found that, *with a stand-alone AGCM,* the simulated precipitation anomaly over south Asia associated with the Eurasia snow anomaly is a factor of 2–3 larger than the observations. Lau and Nath (2000) showed that the Indian Ocean air–sea coupling reduces the monsoon interannual perturbations caused by ENSO. These side evidences suggest that, in the real world, air–sea coupling is possibly working over the Asia–Pacific region to regulate the summer monsoon rainfall toward the climatological mean.

In this study, we primarily focused on the impacts of air–sea coupling on the mean Asian summer monsoon and tried to figure out the underlying physics. Though the improvement of CISO is shown, the comprehensive analyses of the causes need more diagnosis and controlled experiments. This will be deferred to future studies. The impacts of coupling on the transient intraseasonal oscillation are also very significant and partly reported in another paper (Kemball-Cook et al. 2002). Because only one AGCM and one ocean model are used in this study, apparently more research with a variety of AGCMs and ocean models (including OGCMs) are needed to test the hypothesis raised in this study: *air–sea coupling is an important factor in regulating the mean Asian summer monsoon and is missing in the AGCM simulations (AMIP I and II).* To compare the monsoon simulations in two modeling groups [AMIP and Coupled Model Intercomparison Project (CMIP)] will be a very beneficial approach to evaluate the impacts of air–sea coupling. Through this comparison, we will gain more understanding about how the Asian summer monsoon responds to air–sea coupling in different models, and further we may explore the possible different behaviors of the atmospheric parameterization schemes under the stand-alone condition and in the coupled system.

In this study, we have emphasized the possible impacts of air–sea coupling on the simulation of the Asia–Pacific summer monsoon through adjusting SST to the errors of an atmospheric model. Another important issue that deserves more study is how the errors of an ocean model contribute to the ''new equilibrium'' of the coupled system. For our specific case, the stand-alone ocean model driven by the observed atmospheric forces [Oberhuber's (1988) surface winds and solar radiation, and observed surface air temperature is used in the calculations of latent and sensible heat fluxes] actually produce a slightly warm SST bias in the Indian and western Pacific Oceans. We also coupled ECHAM4 with Mission Operations Manager (MOM) ocean GCM without heat flux correction. The Asian summer monsoon in this coupled general circulation model (CGCM) is similar to that in our control run. These suggest that our results are not very sensitive to a specific ocean model used.

Though the simulated Asian summer monsoon in the coupled model looks more realistic than that in the stand-alone model, the coupled results still have considerable discrepancies with the observations. Therefore, we do not consider air–sea coupling as a panacea for all the problems of Asian summer monsoon simulations in stand-alone AGCMs. Studies on land surface processes, cumulus parameterization, and cloud–radiation interactions are needed to further improve the monsoon simulations in AGCMs and coupled models. If we can evaluate those schemes in the coupled mode, our understandings of monsoon dynamics should be improved considerably, because in nature the monsoon is interacting with the underlying oceans. The possible impacts of the regional air–sea coupling modes in the Indian and western Pacific Oceans, for example, Indian dipole mode and western Pacific anticyclone mode (Wang et al. 2000), on the simulation of Asia–Pacific monsoon climatology are under investigation.

Acknowledgments. The authors appreciate Drs. L. Bengtsson, E. Roeckner, L. Dumenil, and U. Schulzweida at the Max-Planck-Institute for Meteorology in Germany for their kind help in the implementation of the ECHAM4 AGCM at IPRC. The first author thanks Dr. H. Annamalai for the discussions with him and his comments on an earlier version of the manuscript. He also extends his thanks to three anonymous reviewers for their stimulating questions and comments, which lead to significant improvements of the manuscript. The authors also acknowledge the support by NOAA/PACS program. The International Pacific Research Center (IPRC) is partly sponsored by the Frontier Research System for Global Change.

REFERENCES

Anathakrishnan, R., and M. K. Soman, 1988: The onset of the southwest monsoon over Kerala: 1901–1980. *J. Climatol.,* **8,** 283–296.

Barnett, T. P., L. Dumenil, U. Schlese, E. Roeckner, and M. Latif, 1989: The effect of Eurasian snow cover on regional and global climate variations. *J. Atmos. Sci.,* **46,** 661–685.

Dumenil, L., and E. Todini, 1992: A rainfall-runoff scheme for use in the Hamburg climate model. *Advances in Theoretical Hydrology, A Tribute to James Dooge,* European Geophysical Society Series on Hydrological Sciences, Vol. 1, Elsevier Press, 129–157.

Fu, X., and B. Wang, 2001: A coupled modeling study of the annual cycle of Pacific cold tongue. Part I: Simulation and sensitivity experiments. *J. Climate,* **14,** 765–779.

Gadgil, S., and S. Sajani, 1998: Monsoon precipitation in the AMIP runs. *Climate Dyn.,* **14,** 659–689.

Gaspar, P., 1988: Modeling the seasonal cycle of the upper ocean. *J. Phys. Oceanogr.,* **18,** 161–180.

Hahn, D., and S. Manabe, 1975: The role of mountains in the south Asian monsoon circulation. *J. Atmos. Sci.,* **32,** 2461–2463.

Ju, J., and J. M. Slingo, 1995: The Asian summer monsoon and ENSO. *Quart. J. Roy. Meteor. Soc.,* **121,** 1133–1168.

Kang, I.-S., C.-H. Ho, Y.-K. Lim, and K.-M. Lau, 1999: Principal modes of climatological seasonal and intraseasonal variations of the Asian summer monsoon. *Mon. Wea. Rev.,* **127,** 322–340.

——, K. Jin, B. Wang, and K.-M. Lau, 2002: Intercomparison of the climatological variations of Asian summer monsoon rainfall simulated by 10 GCMs. *Climate Dyn.*, in press.

Kawamura, R., and T. Murakami, 1998: Baiu near Japan and its relation to summer monsoons over southeast Asia and the western North Pacific. *J. Meteor. Soc. Japan,* **76,** 619–639.

Kemball-Cook, S., B. Wang, and X. Fu, 2002: Simulation of the intraseasonal oscillation in the ECHAM-4 model: The impact of coupling with an ocean model. *J. Atmos. Sci.*, **59,** 1433–1453.

Kuo, H. L., and Y. F. Qian, 1981: Influence of the Tibetan Plateau on cumulative and diurnal changes of weather and climate in summer. *Mon. Wea. Rev.*, **109,** 2337–2356.

Lau, K.-M., and P. H. Chan, 1986: Aspects of the 40–50 day oscillation during the northern summer as inferred from outgoing longwave radiation. *Mon. Wea. Rev.*, **114,** 1354–1367.

Lau, N. C., and M. J. Nath, 2000: Impact of ENSO on the variability of the Asian–Australian monsoons as simulated in GCM experiments. *J. Climate,* **13,** 4287–4309.

McCreary, J. P., P. K. Kundu, and R. L. Molinari, 1993: A numerical investigation of dynamics, thermodynamics and mixed-layer processes in the Indian Ocean. *Progress in Oceanography,* Vol. 31, Pergamon, 181–244.

Meehl, G. A., 1987: The annual cycle and interannual variability in the tropical Pacific and Indian Ocean regions. *Mon. Wea. Rev.*, **115,** 27–50.

Miller, M. J., T. N. Palmer, and R. Swinbank, 1989: Parameterization and influence of sub-grid scale orography in general circulation and numerical weather prediction models. *Meteor. Atmos. Phys.*, **40,** 84–109.

Murakami, T., and B. Wang, 1993: Annual cycle of equatorial east–west circulation over the Indian and Pacific Oceans. *J. Climate,* **6,** 932–952.

——, J. Matsumoto, and A. Yatagai, 1999: Similarities as well as differences between summer monsoons over southeast Asian and the western North Pacific. *J. Meteor. Soc. Japan,* **77,** 887–906.

Nakazawa, T., 1992: Seasonal phase lock of intraseasonal variation during the Asian summer monsoon. *J. Meteor. Soc. Japan,* **70,** 597–611.

Nordeng, T. E., 1995: Extended versions of the convective parameterization scheme at ECMWF and their impact on the mean and transient activity of the model in the tropics. ECMWF Research Dept. Tech. Memo., 206, European Centre for Medium-Range Weather Forecasts, Reading, United Kingdom, 41 pp.

Oberhuber, J. M., 1988: An atlas based on the COADS dataset: The budgets of heat, buoyancy, and turbulent kinetic energy at the surface of the global ocean. Max-Planck-Institute for Meteorology Rep. 15, 20 pp. plus plates.

Rasmusson, E. M., and T. H. Carpenter, 1983: The relationship between eastern equatorial Pacific sea surface temperatures and rainfall over India and Sri Lanka. *Mon. Wea. Rev.,* **111,** 354–384.

Rodwell, M. J., and B. J. Hoskins, 1995: A model of the Asian summer monsoon. Part II: Cross-equatorial flow and PV behavior. *J. Atmos. Sci.,* **52,** 1341–1356.

Roeckner, E., and Coauthors, 1996: The atmospheric general circulation model ECHAM-4: Model description and simulation of present-day climate. Max-Planck-Institute for Meteorology Rep. 218, 90 pp.

Shukla, J., and M. J. Fennessy, 1994: Simulation and predictability of monsoons. *Proc. of the Int. Conf. on Monsoon Variability and Prediction,* Tech. Rep. WCRP-84, Geneva, Switzerland World Climate Research Programme, 567–575.

Sperber, K. R., and T. N. Palmer, 1996: Interannual tropical rainfall variability in general circulation model simulations associated with the atmospheric model intercomparison project. *J. Climate,* **9,** 2727–2750.

Stendel, M., and E. Roeckner, 1998: Impacts of horizontal resolution on simulated climate statistics in ECHAM4. Max-Planck-Institute for Meteorology Rep. 253 Hamburg, 120 pp.

Taylor, K. E., D. Williamson, and F. Zwiers, 2000: The sea surface temperature and sea-ice concentration boundary condition for AMIP II simulations, PCMDI Rep. 60, Program for Climate Model Diagnosis and Intercomparison, Lawrence Livermore National Laboratory, Livermore, CA, 25 pp. [Available online at http://www-pcmdi.llnl.gov/amip/AMIP2EXPDSN/BCS/amip2bcs.html.]

Tiedtke, M., 1989: A comprehensive mass flux scheme for cumulus parameterization in large-scale models. *Mon. Wea. Rev.,* **117,** 1779–1800.

Wang, B., and X. Xu, 1997: Northern Hemisphere summer monsoon singularities and climatological intraseasonal oscillation. *J. Climate,* **10,** 1071–1085.

——, and X. Fu, 2001: Physical processes determining the rapid reestablishment of the equatorial Pacific cold tongue/ITCZ complex from March to May. *J. Climate,* **14,** 2250–2265.

——, T. Li, and P. Chang, 1995: An intermediate model of the tropical Pacific Ocean. *J. Phys. Oceanogr.,* **25,** 1599–1616.

——, R. Wu, and X. Fu, 2000: Pacific–east Asian teleconnection: How does ENSO affect east Asian climate? *J. Climate,* **13,** 1517–1536.

Webster, P. J., 1987: The elementary monsoon. *Monsoons,* J. S. Fein and P. L. Stephens, Eds., John Wiley, 269–330.

Xie, P., and P. A. Arkin, 1997: Global precipitation: A 17-year monthly analysis based on gauge observations, satellite estimates, and numerical model outputs. *Bull. Amer. Meteor. Soc.,* **78,** 2539–2558.

Yang, S., P. J. Webster, and M. Dong, 1992: Longitude heating gradient: another possible factor influencing the intensity of the Asian summer monsoon circulation. *Adv. Atmos. Sci.,* **9,** 397–410.